Polymer 50 (2009) 4128–4138

Contents lists available at ScienceDirect

Polymer

journal homepage: www.elsevier.com/locate/polymer

Fabrication and characterization of poly(L-lactic acid) 3D nanofibrous scaffolds with controlled architecture by liquid–liquid phase separation from a ternary polymer–solvent system

Liumin He [a,c], Yanqing Zhang [b], Xiang Zeng [b], Daping Quan [a,*], Susan Liao [c], Yuanshan Zeng [b], Jiang Lu [a], S. Ramakrishna [c]

[a] Institute of Polymer Science, School of Chemistry and Chemical Engineering, BME Center, State Key Laboratory of Optoelectronic Materials and Technologies, Sun Yat-sen University, 135 XinGang Xi Road, Guangzhou 510275, China
[b] Department of Histology and Embryology, Zhongshan School of Medicine, Sun Yat-sen University, Guangzhou 510080, China
[c] Nanoscience and Nanotechnology Initiative, Division of Bioengineering, National University of Singapore, 9 Engineering Drive 1, Singapore 117576, Singapore

ARTICLE INFO

Article history:
Received 19 December 2008
Received in revised form
9 June 2009
Accepted 15 June 2009
Available online 18 June 2009

Keywords:
Phase separation
Nanofibrous scaffold
Crystalline form

ABSTRACT

Poly(L-lactic acid) (PLLA) three-dimensional (3D) scaffold with macro/micropores and nanofibrous structure was fabricated by phase separation from a ternary PLLA/dioxane/water system. The pore size was mainly determined by the coarsening effects in the phase separation process, while the nanofibrous structure was due to the formation of PLLA microcrystallite domains in the gelation process. Increasing the gelation temperature or the content of water in the mixed solvent system, the pore size definitely increased and macropores up to 300 μm were observed. However, coalescence of nanofibers occurred, even platelet-like structure appeared at gelation temperatures higher than 12 °C or the proportion of water exceeded 12%. X-ray diffraction (XRD) and Differential Scanning Calorimetry (DSC) analyses demonstrated that the crystallinity degree increased with increasing the gelation temperature or the non-solvent volume ratio in the mixed system. Moreover, the results indicated that α′ was mainly corresponding to the nanofibers structure, while α crystal was detected in the platelet-like structure. Scanning electron micrograph (SEM) and methyl thiazolyl tetrazolium (MTT) assays indicated that the nanofibrous scaffold provided a better attachment and viability of MSCs (rat derived mesenchymal stem cells) than the platelet-like scaffold.

1. Introduction

In the strategy of tissue engineering, porous three-dimensional (3D) scaffold [artificial extracellular matrix (ECM)] serves as a temporary environment for cellular attachment, migration, proliferation and differentiation. The scaffolds also play a major role in guiding new tissue formation in three dimensions [1,2]. Therefore the nature of scaffold as well as the chemical and physical properties of the material are critical to the desired condition for tissue formation [3,4].

Synthetic polymers, including polylactic acid (PLA), polyglycolic acid (PGA), polycaprolactone (PCL) and their copolymers have been extensively studied to fabricate scaffolds because of their advantages of availability, ease of processing, adjustable degradation, low inflammatory response [5]. Meanwhile, a lot of fabricating techniques have been well-documented, such as salt leaching [6,7], expansion in high pressure gas [8], emulsion freeze-drying [9], 3D printing [10–12] and phase separation [13,14], which have been developed to generate highly porous polymer scaffolds. However, different dimensional scales require considering in the scaffold design and fabrication [15]: the large scale of centimeter and millimeter decides the shape and dimension of the engineering tissue; the scale of micron (from tens to 100 μm) adapts the ingrowth and growth of cells; the scale of nanometer (from tens to hundreds nanometers) controls cellular attachment and function, the ingrowth of capillary, neuron extension and conjunction. Thus 3D scales and hierarchical structures control the growth process of newly regenerating tissue.

Recently, more and more nanofibrous scaffolds are being exploited for medical applications. Attributing to a high surface-to-volume ratio, the fibrous structure of collagen have been found to play a positive role in cell attachment, proliferation, and differentiation function in tissue cultures, and such mimicking structure may lead to engineered tissue more closely resembling native

* Corresponding author. Tel.: +86 20 8411 4030; fax: +86 20 8411 2245.
E-mail address: cesqdp@mail.sysu.edu.cn (D. Quan).

0032-3861/$ – see front matter © 2009 Elsevier Ltd. All rights reserved.
doi:10.1016/j.polymer.2009.06.025

tissues [16]. Three basic approaches have emerged to fabricate scaffolds with nanofibrous structure up to now: self-assembly, electrospinning and thermally induced phase separation (TIPS) [17,18]. Ma and Zhang pioneered the preparation of 3D nanofibrous scaffolds through spinodal liquid–liquid phase separation and a consequential crystallization of the polymer-rich phase [19]. This 3D continuous fibrous network with a fiber diameter of 50–500 nm has shown to act as a positive cue to support neurite outgrowth [20], selectively enhance protein adsorption [21] and promote osteoblast differentiation and biomineralization [22].

The phase separation technique is based on thermodynamic demixing of a homogeneous polymer–solvent system into a polymer-rich phase and a polymer poor phase, usually by either cooling the solution below a bimodal solubility curve or exposure of the solution to additional immiscible solvent [19,23,24]. The crucial step to create this unique fibrous matrix structure was the gelation of polymer–solvent system. In PLLA/THF binary system, gelation sequent after the phase separation was driven by thermal energy. The gelation due to the formation of PLLA microcrystalline domains acted as crosslink to stabilize the mixture system, preventing further phase separation. Thus the liquid solvent-rich droplets would have little change during the gelation and the resultant pore size was mainly determined by the polymer concentration. Moreover, shrinkage of the resultant scaffolds would accompany the solvent exchanging process [20]. Therefore, micropores of small size were resulted from the PLA/THF system and it was difficult to simultaneously obtain nanofiber and macro/microporous structure. Porogen materials should be added into the system during process in order to obtain macro/microporous architectures [25].

In the multiple solvent systems, non-solvent-induced liquid–liquid phase separation would occur accompanying the thermally induced phase separation when cooling the mixed system [14,26]. Solvents with relatively high freezing points would crystallize and freeze when quenching the system to a low temperature. Thus porous structures can be created together with nanofibers after the evaporation of solvents [23,24]. Coarsening effects have usually been utilized to control pore size of the scaffold prepared by the technique of TIPS [27,28]. Therefore, it would be possible to use the pore enlargement which was affected by the quenching temperature, quenching depth, aging time and the proportion of water in the PLLA/dioxane/water ternary system to generate open macro/micropores besides nanofibrous network. It is also of great importance to pay attention to study the control of multi-scale size from nano scale to micro/macro-scale in the fabrication of the scaffold using TIPS technique.

To test our hypothesis, we modified the technique of phase separation and prepared PLLA scaffold with highly interconnected macro/microporous structure and nanofibrous walls from PLLA/dioxane/water ternary system. The scaffold morphologies were controlled by optimizing parameters during the fabrication process. The crystallization properties of PLLA scaffold, which have not been attracted enough academic attentions in the existing research, were elucidated by X-ray diffraction (XRD) and Differential Scanning Calorimetry (DSC). Finally, rat derived mesenchymal stem cells (MSCs) were selected to evaluate the influences of the scaffold architecture on the cell adhesion and viability.

2. Experimental details

2.1. Materials

PLLA with an inherent viscosity of 1.75 dl/g was synthesized in our laboratory. All reagents were used directly without any further purification.

2.2. Fabrication of 3D PLLA scaffolds

The nanofibrous scaffolds were fabricated by liquid–liquid phase separation from a PLLA/dioxane/water ternary system. Briefly, 5% (*W/V*) clear solution was obtained by dissolving a certain PLLA in dioxane/water mixed solvents with different volume ratios (90/10, 88/12, 86/14) at 60 °C. Subsequently, it was quenched to a designed temperature (0 °C, 4 °C, 8 °C, 12 °C, 16 °C, 20 °C) and aged for 2 h, followed by quenching to −40 °C for another 2 h to freeze the samples completely. The scaffold was obtained after lyophilization under 0.940 mbar at −10 °C for five days (ALPHA2-4 freeze dryer: Martin Christ Gefriertrocknungsanlagen Gmbh).

To study the influence of aging in the gel status on scaffold morphology, 5% (*W/V*) PLLA/dioxane/water solution was directly quenched to −40 °C and maintained for 2 h followed by lyophilization under 0.940 mbar at −10 °C for five days.

For comparison, PLLA nanofibrous scaffold was also prepared from PLLA/THF system. 5% (*W/V*) clear solution was obtained by dissolving PLLA into THF at 60 °C. The solution was quenched to −30 °C and maintained for 2 h, soon during which period, a gel was formed from the solution. After that the gel was immersed into cold ultrapure water (4 °C) for 2 days for leaching out the solvent by changing the water four times per day. The resultant sample was freeze-dried under 0.940 mbar at −10 °C for five days.

2.3. Characterization of PLLA scaffolds

The morphology of scaffolds was observed by Scanning Electron Microscope (JSM-6380LA-JEOL Ltd, Japan) at an accelerated voltage of 15 KV.

Thermal properties were analyzed by Differential Scanning Calorimeter (MDSC2910: TA instrument, USA) in a temperature range from 20 °C to 220 °C with a heating rate of 10 °C/min. The first heating was performed for the analysis.

The degree of crystallinity (X_c) was calculated according to equation (1):

$$X_c = (\Delta H_m/\Delta H_m^0) \times 100\% \quad (1)$$

ΔH_m is the heat of fusion, ΔH_m^0 is the heat of fusion for 100% crystalline PLA, 93.6 J/g [29].

The crystal structure of PLLA scaffold was characterized through XRD (D/MAX 2200 VPC: RIGAKU Ltd, Japan) with Cu Kα source. The analysis was performed in the 2θ range of 5–40° at a scanning rate of 1.5°/min.

The size of crystallites was calculated according to Scherrer formula:

$$L_{hkl} = K\lambda/(\beta\cos\theta) \quad (2)$$

here L_{hkl} is the crystallite size; K is Scherrer constant, $K = 0.9$; λ is the wavelength of the *radiation*, $\lambda = 1.5406$; β is the full width at half maximum (FWHM) of the reflection.

2.4. Protein adsorption to scaffolds

PLLA scaffolds of two different pore morphologies, nanofibrous structure and micro-scaled platelet-like lamellas, were first wetted by soaking in 100% ethanol for an hour and subsequently in phosphate buffered saline (PBS) for 30 min thrice. The scaffolds were then incubated in PBS overnight at room temperature. The wetted scaffolds were incubated in 0.5% (*w/v*) bovine serum albumin (Shanghai Bo'ao Biological Technology Co., Ltd. Shanghai, China) solutions in PBS for 4 h. After the incubation, the scaffolds were removed from the protein solution and then washed in PBS thrice

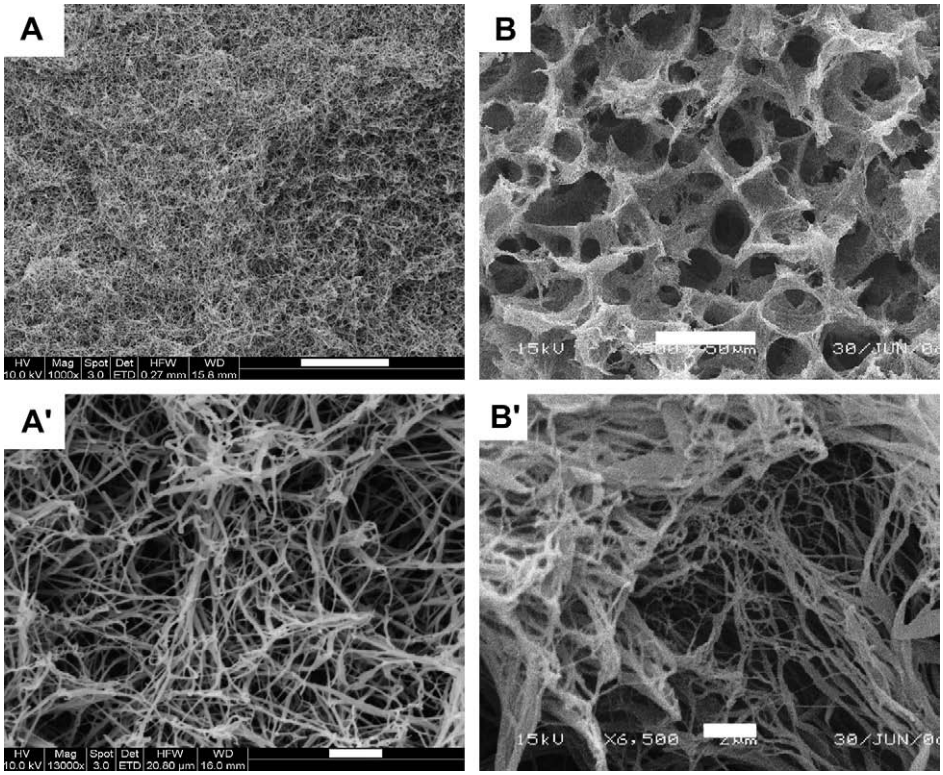

Fig. 1. Scanning electron micrographs of PLLA porous scaffolds with nanofibers prepared from 5% (*W/V*) PLLA solution in THF at $T_{gel} = -30\ ^{\circ}C$ (A,A′) and 5% (*W/V*) PLLA in 88/12 dioxane/water at $T_{gel} = 12\ ^{\circ}C$ (B,B′). Scale bar in A, B = 50 μm; A′,B′ = 2 μm.

(1 × 1 h) to remove free and loosely adsorbed proteins. The total amount of protein absorbed to the scaffolds was measured using MicroBCA assay (Pierce, Rockford, IL).

2.5. Isolation and culture of MSCs from adult rat bone marrow

Male GFP transgenic Sprague–Dawley rats [“green rat CZ-004” SD TgN (act-EGFP) OsbCZ-004, weighing 100 g] of four weeks old were sacrificed by cervical dislocation after inhalation of diethylether. Bone marrow progenitor cells were collected by flushing femurs with low glucose Dulbecco’s Modified Eagle’s Medium (L-DMEM, GIBCO) supplemented with 10% fetal bovine serum (FBS, TBD, Zhanchen) and antibiotics (100 U/ml penicillin and 100 U/ml streptomycin). The progenitor cells were seeded at 1.0×10^7 cells/ml into a 50 ml tissue culture flask with L-DMEM, incubated at 37 °C in a humidified atmosphere containing 5% CO_2. After 72 h, nonadherent cells were removed by changing the culture medium. Dissociate the cells with 0.25% trypsin supplemented with 0.02% EDTA when the adherent MSCs grew to 80% confluence (till day 7th, defined as MSCs of passage 0). Then the cells were cultivated at 1.0×10^4 cells/cm^2 in T-75 flasks and were expanded through successive passages when they reached 80% confluence once more. MSCs of passages 3–6 were used for following experiments.

2.6. MSCs cultured on PLLA scaffold

The PLLA scaffold was cut to $1.5 \times 1.5 \times 1.5$ mm^3 in volume, and sterilized with 75% alcohol for 10 min, followed by washing with 0.01 M PBS thrice. Rat derived MSCs were dissociated with trypsin–EDTA for 2 min, resuspended in the L-DMEM medium at a target concentration of approximately 5.0×10^5 cells/ml, and then administered each side of the PLLA scaffold with a 5 μl micro-injector. The volume of the cell suspension was 1 μl with each side. Incubate cell-loaded scaffolds in L-DMEM medium with 10% FBS for 72 h prior to microscopic evaluation *in vitro*. At intervals of 12 h, day 1 and day 7, the PLLA scaffolds loaded with cells were fixed in

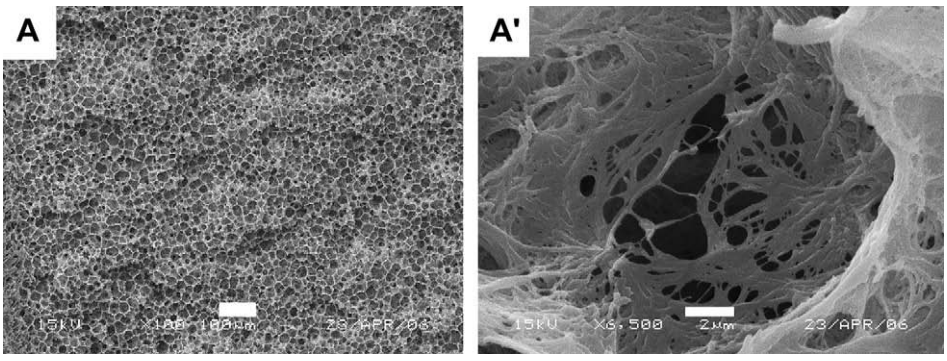

Fig. 2. Scanning electron micrographs of PLLA scaffolds prepared from 5% (*W/V*) PLLA in 88/12 dioxane/water without aging (A, A′). Scale bar in A = 100 μm; in A′ = 2 μm.

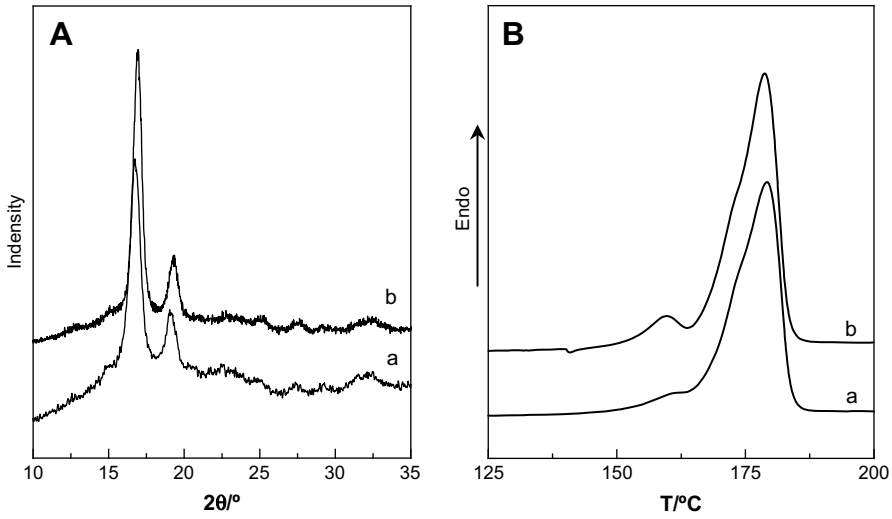

Fig. 3. X-ray diffraction patterns (A) and DSC thermogram (B) of PLLA scaffolds prepared without aging (a) and with aging for 2 h in the gel status at 12 °C (b). The volume ratio of dioxane/water was 88/12 and polymeric concentration was 5% (*W/V*).

4% paraformaldehyde for 0.5 h. After rinsed by PBS for 3 times (3 × 5 min), the samples were dehydrated with a graded concentration (50–100% *V/V*) of ethanol. Subsequently, the samples were kept in a fume hood for air drying. The samples were finally mounted onto a stub and coated with gold using sputter coating for the observation of cell morphology by SEM.

2.7. Cell proliferation in two PLLA scaffolds

In order to carry out the MTT Assay, the PLLA scaffolds were cut into small sample (1.5 × 1.5 × 1.5 mm^3), and washed thrice with 0.01 MPBS after sterilization in 70% ethanol for 10 min. MSCs were suspended in the culture medium and plated into PLLA scaffolds prepared at the gelation temperatures of 12 °C and 20 °C at a density of 1.0×10^4 cells/well, referring to "nanofiber" and "platelet" respectively. A cell suspension with the same density was also plated in the 96 well tissue culture plate and was referred to as TCP control. After cell culturing for 12 h, 1 day, 2 days, 3 days, 5 days and 7 days respectively, the samples were treated with 100 μl/well of 1 mg/ml MTT followed by incubation for another 4 h at 37 °C. The supernatant was then discarded and the formazan crystals were solubilized by adding 100 μl of DMSO solution. The plates were kept in room temperature for 10 min and stabilized. The optical density of each well was read at 490 nm using a BIO-RAD Model 550 Microplate Reader (Bio-Rad, USA).

3. Results

3.1. PLLA nanofibrous scaffolds prepared from different solvent systems

Nanofibrous scaffolds fabricated from PLLA/THF and PLLA/dioxane/water are shown in Fig. 1. Compact and symmetrical nanofibers were resulted from PLLA/THF when gelling for 2 h at −30 °C (Fig. 1A, A′). Micropores were clearly visible, the diameters, however, were below 10 μm. In contrast, the matrix with both interconnected micropores and nanofibrous network were obtained from PLLA/dioxane/water (88/12, *V/V*) at 12 °C gelation temperature for 2 h (Fig. 1B, B′). The pore diameter measured from SEM pictures was 50 ± 25 μm, much larger than those prepared from PLLA/THF. The walls of the micropores were composed of nanofibrous network with the fiber diameter ranging from 50 nm to 200 nm. Therefore, the multi-scale porous scaffold with nanofibrous structure can be obtained from liquid–liquid phase separation using PLLA/dioxane/water system.

3.2. The influences of aging in the gel status on the morphologies and the crystallization of PLLA scaffold

Gelation of the PLLA/dioxane/water ternary system played a crucial role in creating the unique nanofibrous structure. Fig. 2 illustrates the morphologies of PLLA scaffolds prepared without aging in the gel status at 12 °C. When the ternary PLLA/dioxane/water system was directly quenched to −40 °C, spherical pores were formed with a diameter of 30 ± 10 μm (Fig. 2A), slightly smaller than the pores in the scaffold when prepared with an aging time of 2 h in the gel status at 12 °C before quenching to −40 °C (see Fig. 1B). The wall of the micropore was not solid and nanofibers were observed even without aging (Fig. 2A′). However, the diameter was not homogenous and mergence of fibers occurred.

XRD and DSC analysis were performed to study the crystallization behaviors of PLLA. Similar XRD patterns were obtained for the PLLA scaffolds prepared with/without aging as shown in Fig. 3A, which had the most intense diffraction peak (*110/200*) and (*111/201*) at 17.0° and 19.4°. Higher peaks were obtained when aging was performed and broad scattering for the amorphous part was observed between 10° and 25° in the XRD pattern of the scaffold prepared without aging. A small melting peak appeared at 159.7 °C prior to the main peak besides the main melting peak (T_m = 178 °C) only when aging was performed. Both the crystallite size (L_{hkl}) and the crystallinity degree (X_c) calculated from XRD and DSC results

Table 1
The size of crystallites and degree of crystallinity (X_c) of PLLA scaffold prepared in 5% (*W/V*) dioxane/water = 88/12 (*V/V*) with/without aging in the gel status at 12 °C.

	Without aging	Aging for 2 h
L_{hkl}/Å (*110/200*)[a]	130.9	145.0
L_{hkl}/Å (*111/201*)[b]	124.9	151.3
X_c[c] (%)	60.6	64.5

[a] The size of crystallites was calculated according to Scherrer formula according to *110/200*.
[b] The size of crystallites was calculated according to Scherrer formula according to *111/201*.
[c] The degree of crystallinity (X_c) was calculated according to equation (1).

were found higher for specimens aging-performed in the gel status than those without aging (Table 1).

3.3. The influences of gelation temperature (T_{gel}) on the morphologies and crystallization of PLLA scaffolds

Fig. 4 displays the morphologic evolution of PLLA scaffolds as a function of T_{gel}. These scaffolds were fabricated from a 5 wt% PLLA solution in 88/12 (*V/V*) dioxane/water at different T_{gel} (0 °C, 4 °C, 8 °C, 12 °C, 16 °C, 20 °C) with aging for 2 h in the gel status. The characteristic macro/micropores were observed in all matrixes. The size of micropores definitely increased with increasing T_{gel} (30 ± 10 μm at $T_{gel} = 0$ °C to $120 \pm 3\,0$ μm at $T_{gel} = 20$ °C). However, higher T_{gel} concomitantly tended to generate more closed pores and gave rise to poor interconnection (Fig. 4E, F). It was interesting that characteristic lacy structures were observed at the T_{gel}s of 0 °C and 12 °C, which were around the freezing points of water and dioxane respectively. The two pore morphologies may be relative to the crystallization and freezing of the solvents around the freezing points.

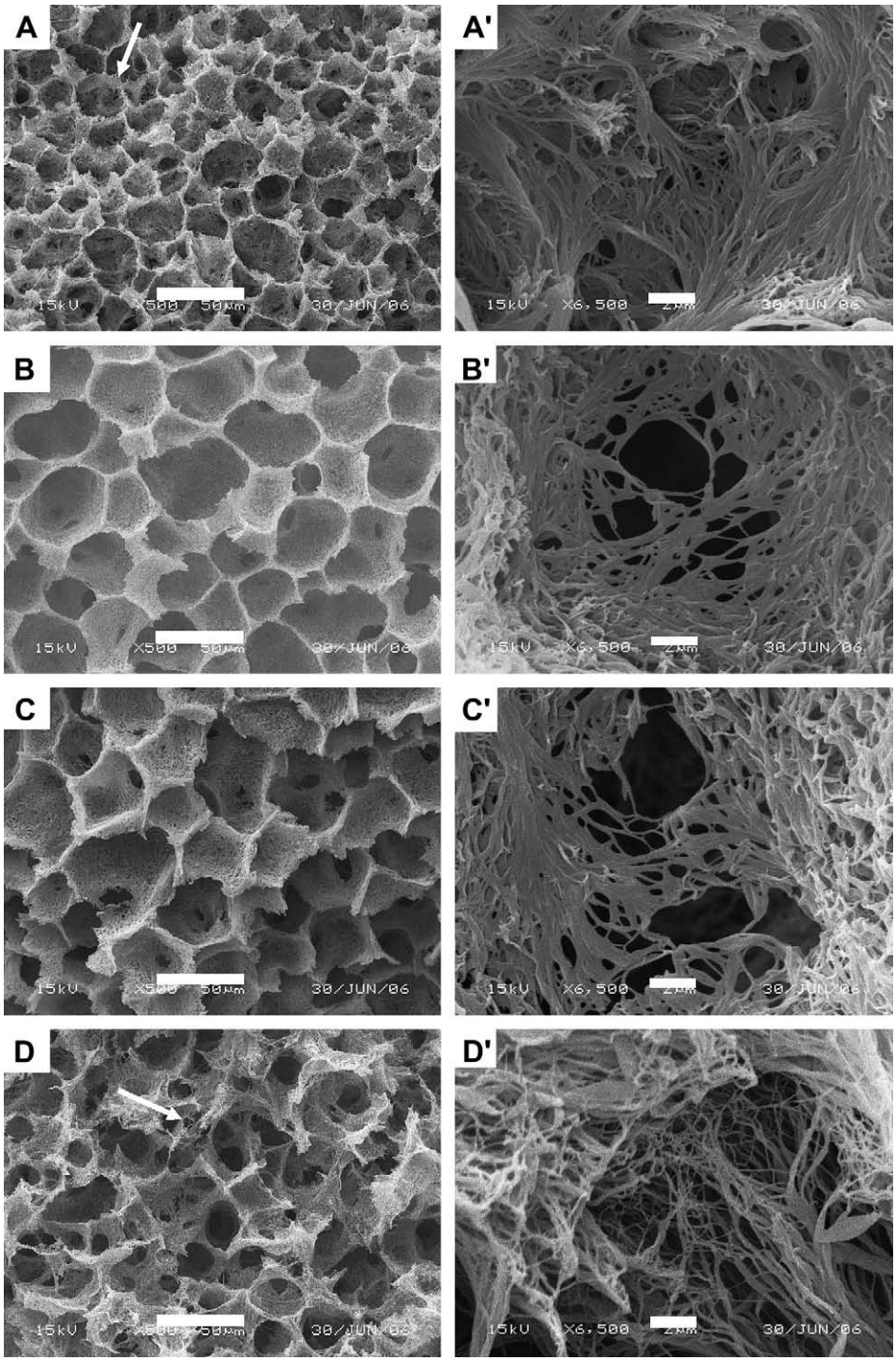

Fig. 4. Scanning electron micrographs of PLLA scaffolds prepared from 5% (*W/V*) PLLA in 88/12 dioxane/water at different gelation temperatures. (A, A′): 0 °C; (B, B′): 4 °C; (C, C′): 8 °C; (D, D′): 12 °C; (E, E′): 16 °C; (F, F′): 20 °C. Scale bar in A, B, C, D = 50 μm; in E, F = 100 μm; in A′, B′, C′, D′, E′, F′ = 2 μm.

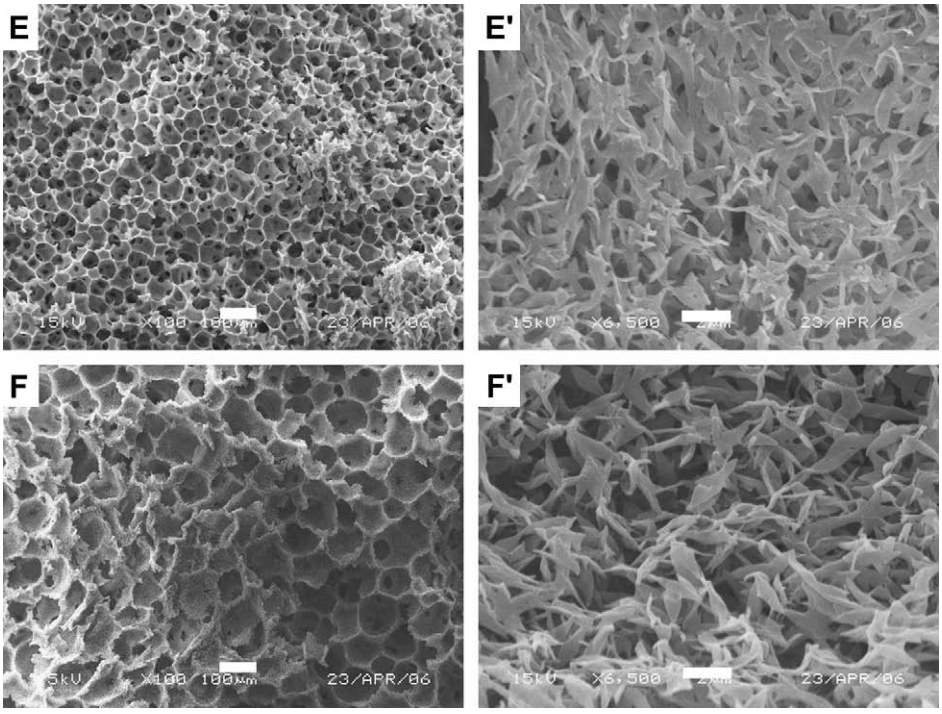

Fig. 4. (*continued*).

SEM photographs of higher magnification showed that evidently different morphologies were formed at different gelation temperatures. The walls of the macro/micropores in the scaffold were composed of nanofibers at low gelation temperatures ($T_{gel} \leq 12$ °C) (Fig. 4A′, 4B′, 4C′, 4D′). However, when the gelation temperature was too low, nanofiber entanglement and mergence occurred (Fig. 4A′). Platelet-like structure was the only structure when T_{gel} increased to 16 °C and 20 °C (Fig. 4E′, 4F′). The size of the platelets was at the micrometer level.

As shown in Table 2, the crystallinity degree and the crystallite size of PLLA scaffold both increased with increasing gelation temperatures analyzed by DSC and XRD analysis. This trend in X_c and L_{hkl} are coincident with the differences in matrix structure and the dependence could be attributed to easier rearrangement of PLLA chains in the solution during crystallization at higher T_{gel} [19].

For $T_{gel} > 12$ °C, besides the two clearly high and narrow peaks for *110*/*200* and *111*/*201* at 2θ values of around 17.0° and 19.4°, many discrete diffraction peaks were found at $2\theta = 12.8°$, 15.1°, 22.6°, 27.5°, 29.3° (Fig. 5A), agreeing well with the orthorhombic crystal structure, which has been assigned as α form modification [30,31]. In contrast, only the two main diffraction peaks for *110*/*200* and *111*/*201* were present for $T_{gel} \leq 12$ °C. A new crystalline form, namely α′ form might be assigned to, which is proposed to a limit disordered crystal having the same 10_3 conformation as in α form but a loose packing manner compared to the α-form [31]. T_{gel} dependence of the melting peak profiles of the DSC curves was also found discretely to vary at 12 °C (Fig. 5B). A single melting peak appeared (curves a, b, c in Fig. 5B) at around 180 °C in the case of lower T_{gel} (0 °C, 4 °C, 8 °C). Double melting peaks (173 °C and 181 °C) appeared in the DSC curves (e and f in Fig. 5B) when PLLA gelled at 16 °C and 20 °C.

Table 2
The crystallite sizes and crystallinity degree (X_c) of PLLA scaffold prepared from 5% (*W*/*V*) in 88/12 (*V*/*V*) dioxane/water at different gelation temperatures.

Gelation temperature/°C	0	4	8	12	16	20
L_{hkl}/Å (*110/200*)[a]	107.7	121.5	125.5	145.0	153.6	162.2
L_{hkl}/Å (*111/201*)[b]	103.1	130.1	135.2	151.3	151.3	143.3
X_c[c] (%)	54.8	63.4	58.1	64.5	67.7	74.2

[a] The size of crystallites was calculated according to Scherrer formula according to *110/200*.
[b] The size of crystallites was calculated according to Scherrer formula according to *111/201*.
[c] The degree of crystallinity (X_c) was calculated according to equation (1).

3.4. The influences of the volume ratio of dioxane/water on the morphologies and crystallization of PLLA scaffolds

The volume ratio of dioxane/water was another influential factor on the morphology of the scaffolds. As shown in Fig. 6, larger size but inhomogeneous pores were tended to generate with increasing amount of water in the solvent mixture (Fig. 6). Especially when the water content increased to 14%, macropores up to 300 μm in diameter could be easily seen with much smaller micropores (tens of microns) between the walls of the large pores. Furthermore, platelet-like pore walls resulted from 14% volume of water replaced the nanofibrous network in the matrixes fabricated with 90/10 and 88/12 ratios of dioxane/water.

The crystallinity degree of scaffold prepared at 86/14 dioxane/water was higher than those at 90/10 and 88/12 dioxane/water (Table 3). However, much lower crystallite sizes at the two dominant diffraction peaks (*110/200* and *111/201*) were obtained at 86/14 dioxane/water than those at 90/10 and 88/12 dioxane/water. According to the aforementioned analysis, the XRD pattern corresponding to α form crystal conformation was found at 86/14 dioxane/water while the XRD pattern at 90/10 dioxane/water was corresponding to the occurrence of α′ form (Fig. 7A). Moreover, the lower melting point at 159 °C disappeared and the double melting peaks (175 °C, 181 °C) appeared in DSC curve at 86/14 dioxane/water (Fig. 7B).

3.5. Adsorption of proteins to the scaffolds

The amount of protein absorbed on PLLA scaffolds of the two characteristic morphologies prepared in this study is shown in

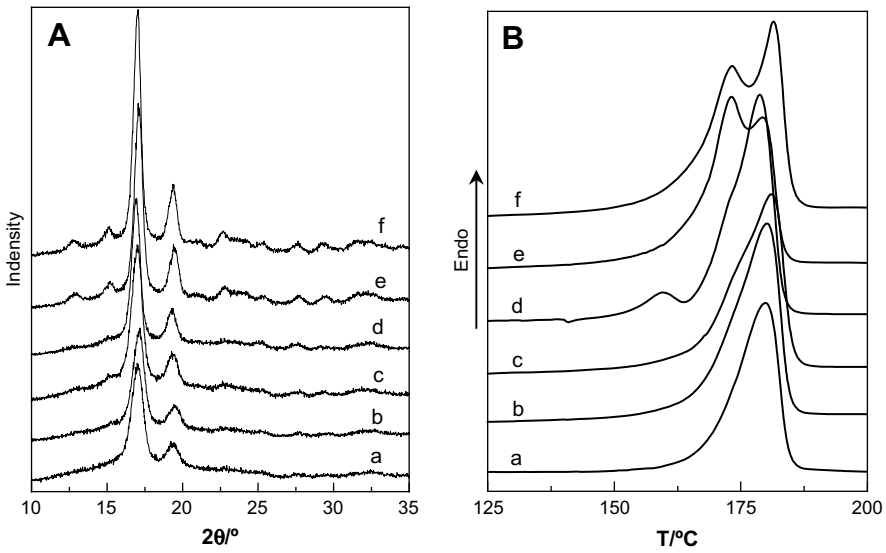

Fig. 5. XRD diagram (A) and DSC thermogram (B) of PLLA scaffolds prepared from 5% (*W/V*) PLLA in 88/12 dioxane/water at different gelation temperatures. (a): 0 °C, (b): 4 °C, (c): 8 °C, (d): 12 °C, (e): 16 °C, (f): 20 °C.

Fig. 8. Much more protein was absorbed on nanofibrous scaffold than the platelet-like scaffold. Quantificationally, the amount of protein absorbed on the nanofibrous scaffold was 1.6 times of that absorbed on the platelet-like scaffold.

3.6. MSC evaluation in two PLLA nano-scaffolds

To examine the influences of the two characteristic structures (nanofibrous structure and micro-scaled platelet-like lamellas) prepared in this study on cell adhesion and proliferation, MSCs were cultured in the scaffolds with different wall structures prepared at the T_{gel} of 12 °C and 20 °C (see Fig. 4D′ and F′ in Fig. 4), referring as nanofiber and platelet respectively. 12 h after seeding, MSCs with polygonal and flattened shape were found to adhere to the nanofibrous scaffold (Fig. 9A). Filaments were observed on the nanofibrous network and the edge of the pore. By one day, MSCs progressively grew throughout the 3D nanofibrous scaffold with more and longer filaments (Fig. 9B). At the same time intervals, spherical cells with seldom filaments were found on the platelet-like scaffold and fewer filaments and smaller cell body (Fig. 9A′, B′) compared with those seeded within the nanofibrous scaffold. The cells extensively spread on both of the nanofibrous scaffold and platelet-like scaffold in the late period post-seeding (Fig. 9C, C′, D, and D′). The cells covered the surface of the pores and pore walls on

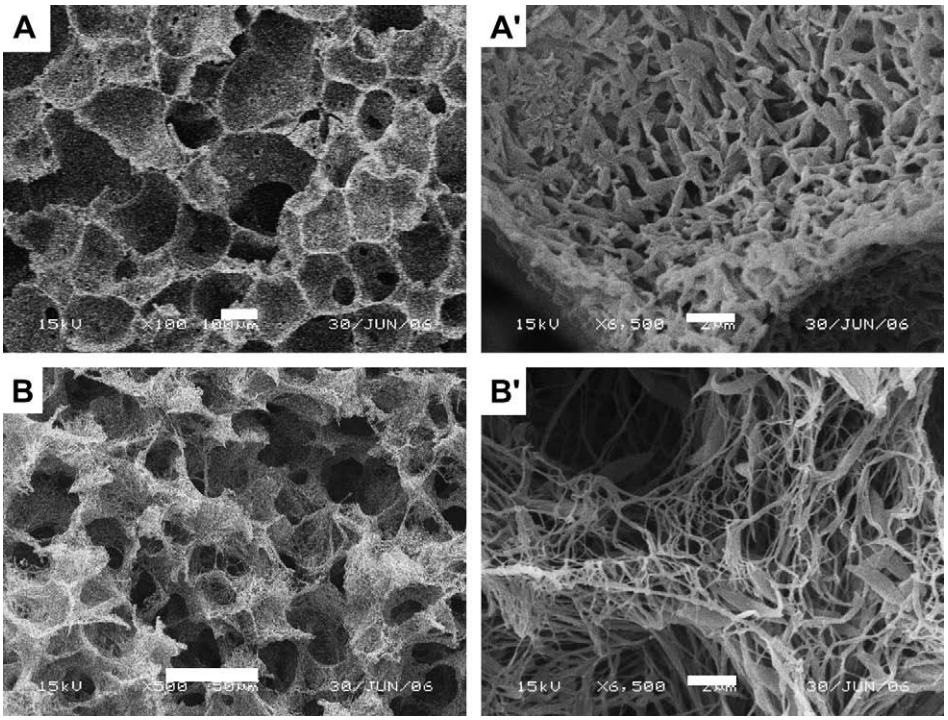

Fig. 6. Scanning electron micrographs of PLLA scaffolds prepared $T_{gel} = 12$ °C with different volume ratio of dioxane/water. (A, A′): 86/14; (B, B′): 90/10. Scale bar in A = 100 μm; B = 50 μm; A′, B′ = 2 μm.

Table 3
The size of crystallites and degree of crystallinity (X_c) of PLLA prepared with different volume ratio of dioxane/water at 12 °C and 5% (*W/V*).

Dioxane/water (v/v)	86/14	88/12	90/10
L_{hkl}/Å (*110/200*)[a]	127.8	145.0	157.0
L_{hkl}/Å (*111/201*)[b]	135.8	151.3	168.5
X_c[c] (%)	66.2	64.5	64.9

[a] The size of crystallites was calculated according to Scherrer formula according to *110/200*.
[b] The size of crystallites was calculated according to Scherrer formula according to *111/201*.
[c] The degree of crystallinity (X_c) was calculated according to the equation (1).

the nanofibrous scaffold with a few filaments extended from cell body and associated with the nanofibers at day 7 (arrows on Fig. 9D). However, the cells spread along the edges between the pores and no filament-like structure was detected on the platelet-like scaffold.

Sustained increasing optical density (OD) value was observed in the MTT assay over the cultivation (Fig. 10). Higher values were obtained in the nanofibrous scaffold than the platelet-like scaffold and the tissue culture plate (TCP) at all intervals. The OD value of platelet-like scaffold was higher than that TCP at 5 days and afterwards.

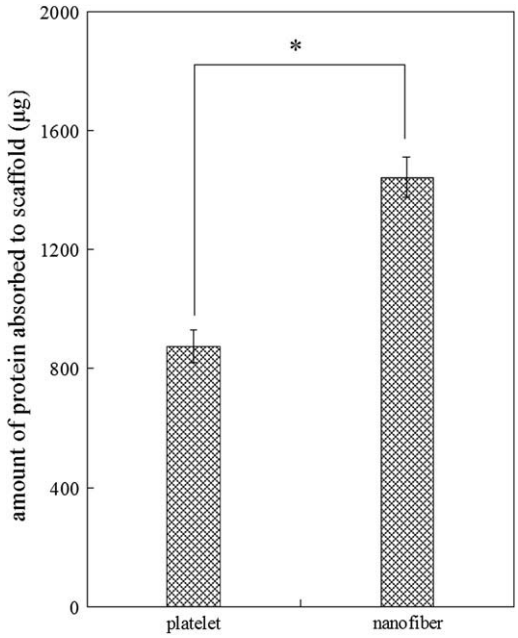

Fig. 8. Amount of adsorbed serum proteins to the scaffolds, platelet: platelet-like scaffold, nanofiber: nanofibrous scaffold.

4. Discussions

A highly porous structure with interconnected spaces plays a key role in scaffolds by offering a supporting base for cell attachment, migration and proliferation [32,33]. Although porous scaffold was formed in the PLLA/THF system, the pore size was quite small because it was mainly determined by the polymer concentration. Thus it was inconvenient to regulate the pore architecture through changing the parameters in the phase separation process [20]. Ma et al. prepared nano-hydroxyapatite/PLLA composite scaffolds from dioxane/water and found that when the water volume was 13% in the mixed solvent system, the scaffolds consisted of large macro-pores in a range of 200–500 μm with loose fibrous walls [34]. They also documented that the diameter of PLLA nanofibers increased with the content of non-solvent in THF/methanol system [35]. However, until now, there is no report concerning the influences of coarsening effect on both of the pore size in the PLLA scaffold and the diameter of the nanofibers simultaneously. Especially, few articles report the relationship between the nanofibrous structure with the crystallization behaviors of PLLA.

The phase separation of a polymer solution can also be considered as a self-assembly process. Instead of the assembling of small molecules, large molecules are easy to aggregate into a new phase from an initially homogeneous one-phase system [36]. In PLLA/dioxane/water system, PLLA microcrystalline resulted from thermal- and non-solvent-induced phase separation accounted for the gelation of the system. This observation was in agreement with previous research when porous scaffolds were prepared from polymer/dioxane/water ternary system [16,27,37]. Therefore, an aging in the gel status was essential for forming nanofibrous network, during which process PLLA chains would rearrange and further crystallize. The coalescence of the solvent-rich drops would also occur when aging was performed in order to reduce the surface tension. This coarsening effect would result in the pore size

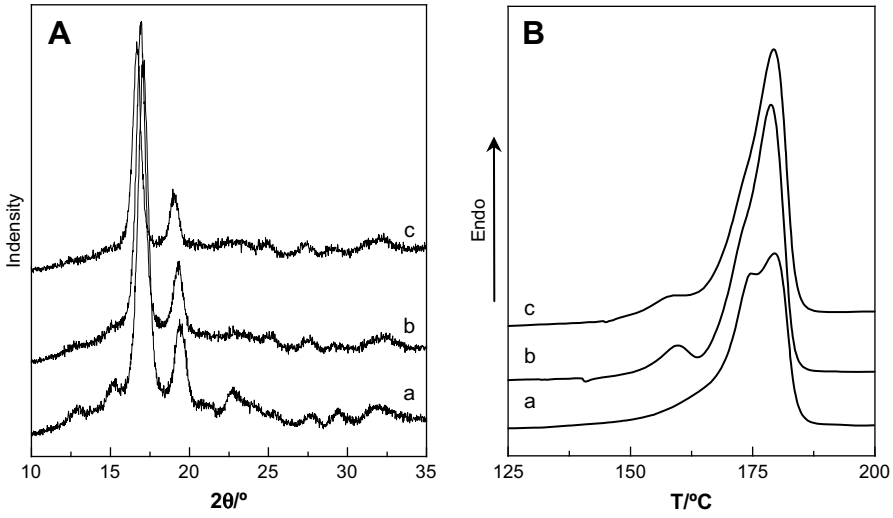

Fig. 7. XRD diagram (A) and DSC thermogram (B) of PLLA scaffolds prepared with different volume ratio of dioxane/water. (a): 86/14, (b): 88/12, (c): 90/10. The gelation temperature was 12 °C and polymeric concentration was 5% (*W/V*).

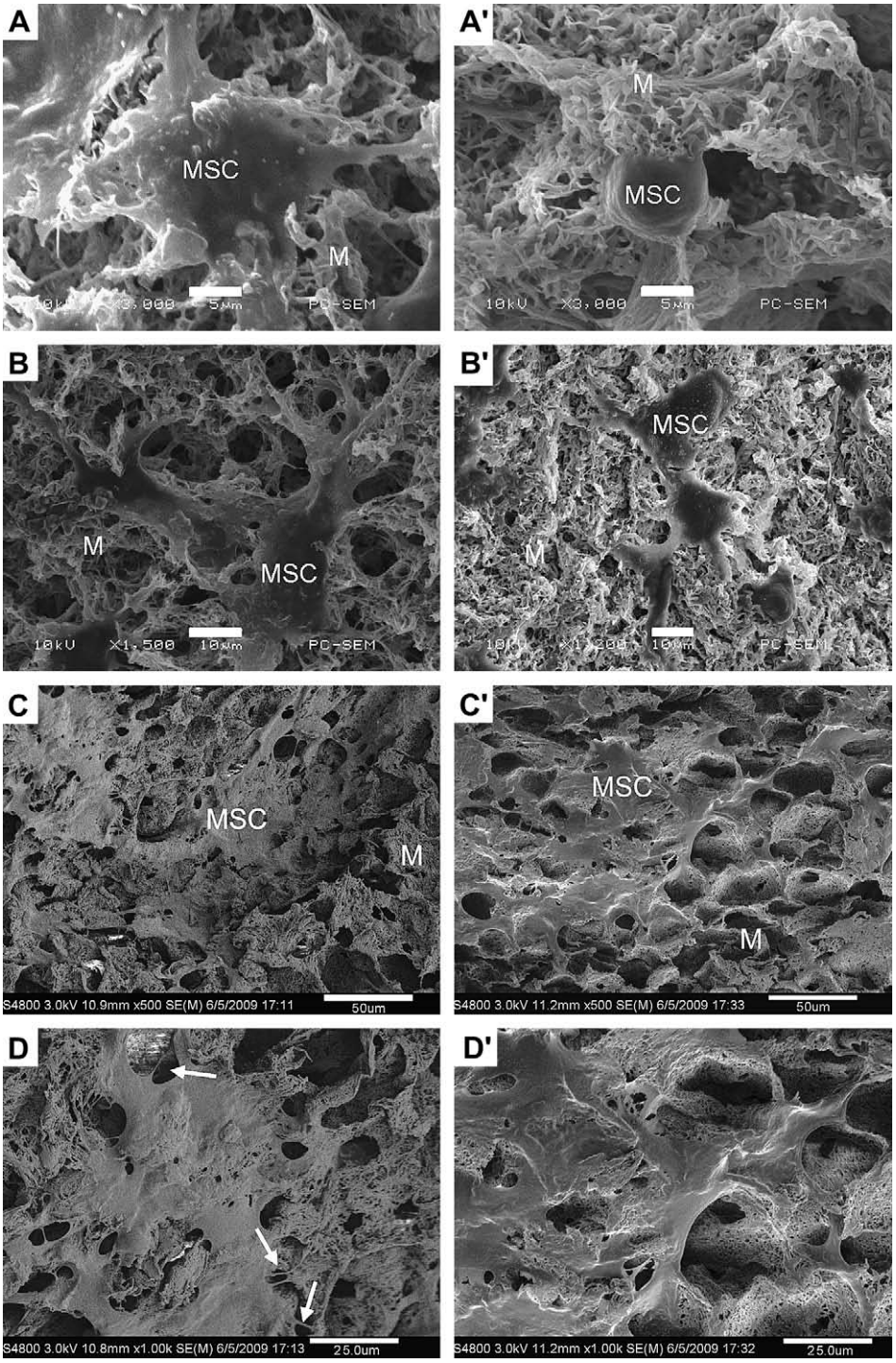

Fig. 9. Scanning electron micrographs of MSCs seeded within the nanofibrous scaffolds (A, B, C, D) and platelet-like scaffolds (A′, B′, C′, D′). (A, A′) 12 h; (B, B′) 1 d; (C, C′, D, D′) 7 d. M: material, MSC: rat derived mesenchymal stem cells. Scale bar in A, A′ = 5 μm; B, B′ = 10 μm; C, C′ = 50 μm, D, D′ = 25 μm.

enlargement [37]. However, the crystallization of PLLA in the gel would restrict the development of phase separation and the coalescence of the solvent-rich drops [16]. This was the reason why the increasing of the pore size was not obvious in our study when aging was performed for 2 h.

In polymeric solution, the morphology development upon spinodal decomposition proceeds through various stages, as indicated in Fig. 11 [38,39]. In the early stage of decomposition a co-continuous structure develops. A dispersed two phase structure would result in the late stage of phase separation due to coarsening effect, yielding fragmented particles and then spherical particles. The shape of the domains is not uniform.

According to the mechanism of liquid–liquid phase separation, the size and morphologies of macro- or micro-pores in the scaffold were affected by the extent of coarsening [14,28]. Since the coarsening effect is a kinetic behavior to minimize the interfacial free energy [28], high quenching temperature (here is T_{gel} in our study) would favor the formation of larger solvent-rich droplets, resulting

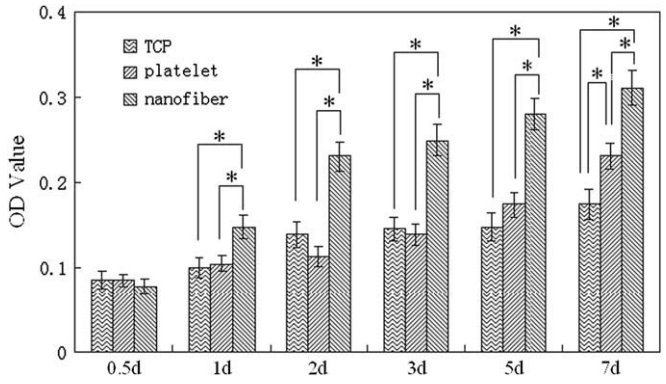

Fig. 10. Growth curves of MSCs cultivated within different scaffolds and tissue culture plate (TCP). TCP: tissue culture plate, platelet: platelet-like scaffold, nanofiber: nanofibrous scaffold.

in pore enlargement. Therefore, such effect was obvious in our study, the micropores (30 ± 10 μm) tended to become macropores (120 ± 30 μm) when the T_{gel} was from 0 °C to 20 °C. However, the pore size was smaller than those in other polymer solution systems reported previously [14,16], which may be due to the crystallization of PLLA in the gel [16]. The coarsening process, however, concomitantly tended to generate more closed pores and gave rise to poor interconnection.

High water content in the system tended to increase the pore size but also give rise to the inhomogeneity (Fig. 6B). This was because high non-solvent volume fraction deteriorated the dissolvability of polymer, a weaker polymer–diluent interaction and lowered viscosity in the cosolvent system might induce the formation of polymer poor phase with greater droplet domains [40,41]. In addition, the gradual addition of water would increased the gelation point [16], thus resulted in a larger quench depth which allowed further reduction of the interfacial free energy between two phases separated at earlier stage of coarsening process, and the formation of macropores (up to 300 μm) in addition to the micropores [14,34]. Therefore, the enlarged pore sizes with increasing water content were most likely due to the combined effects of weaker polymer–diluent interaction, larger quenching depth, and lowered viscosity in the cosolvent system [14].

The morphology of pore was found to have a strong T_{gel} dependence, which was in agreement with the dependences of crystallite size and crystallinity degree. Similar to PLLA/THF system, nanofibrous structure could be formed at a low T_{gel} in the PLLA/dioxane/water system, while high T_{gel} would give rise to the formation of platelet-like structure. Accordingly, different phase separation mechanisms may account for the evident different morphologies. Ma hypothesized that nanofibers were formed by spinodal liquid–liquid phase separation of the polymer solutions and consequential crystallization of the polymer-rich phase, while the platelet-like structure was formed due to the aggregates of many single crystals through a crystal nucleation and growth mechanism [19]. The formation of nanofibrous structure was related not only to the liquid–liquid phase separation but also to the crystallization kinetics of PLLA, which was affected by the cooling rate. Since single crystals might grow to form platelet-like structure at a slow cooling rate, a fast cooling rate is needed to avoid polymer crystal nucleation and growth in order to obtain a uniform nanofiber network. Meanwhile, the crystallization of the solvents with high freezing point would further limit the polymer crystal, thus the fibrous structure was obtained when PLLA/dioxane/water gelled at a range of 4 °C–12 °C.

Different crystalline forms were also found to be corresponding to the different pore structures: nanofibers had form crystal while platelet-like structure had α form. Since α′ form is proposed to a limit disordered crystal which has the same 10_3 conformation as in α form but a loose packing manner compared to the α-form, we hypothesize that PLLA chain arrangement is limited at lower T_{gel} due to lower energy plus solvent molecules freeze. When gelling at high temperatures (16 °C and 20 °C), the solvent was liquid and high energy made the arrangement easy. New diffraction peaks appeared at $2\theta = 12.8°$, 15.1°, 22.6°, 27.5°, 29.3° in the XRD patterns indicating that the imperfect microcrystallite developed to perfect crystallite. Meanwhile, single melting peaks in the DSC curves showed double peaks when T_{gel} increased to 16 °C and 20 °C which may be due to lamellar thickening and crystal perfecting [31,42].

The crystallinity degree was also found to increase with water content in the mixed solvents. The crystalline, however, became smaller. We presumed that more microcrystallines were formed in this coarsening process due to higher non-solvent content. Thus higher crystallinity degree at high water content was resulted from crystal nucleation rather than growth. α form crystal and double melting peaks only appeared in the XRD pattern and DSC curve for platelet-like structure prepared at 86/14 dioxane/water, while the α′ form crystal and single peak was detected for nanofibers prepared at 90/10 dioxane/water.

From the analysis above, we can conclude that the coarsening effects have dual influences on the fabrication of multi-scale nanofibrous scaffold. Larger pores tended to be formed in the coarsening process, which, on the other hand, would facilitate the occurrence of platelet-like structure through crystal nucleation and growth. High X_c at high T_{gel} is mainly relative to the crystal growth, while the increase of X_c with the amount of water in the cosolvent system is mostly determined by the nucleation effects. Both of the coarsening processes resulted in α crystal. Although the mechanism of fibrous texture formation by TIPS is not fully understood until now, the crystallization of PLLA in the polymer-rich phase would present an explanation for the formation of the fibrous structure [19,34]. In this study, a moderate crystallization of PLLA, which resulted in α′ form crystal, may account for the nanofibrous structure. Excessively low or high crystallization could not lead to uniform nanofibrous network [19,23]. The morphology of the resultant scaffold was determined by PLLA crystallization and phase separation process. It is possible to achieve a macro/microporous and nanofibrous structure in the scaffold through optimizing various parameters. A relatively narrow gelation temperature range (4 °C–12 °C), appropriate ratios of cosolvent are essential in the PLLA/dioxane/water ternary system.

Because the fiber diameter in the PLLA nanofibrous scaffold was at nano scale, a higher specific surface was obtained for the nanofibrous scaffold than that for the platelet-like scaffold. Therefore, more proteins were absorbed in the nanofibrous scaffold, such a scaffold may provide a more favorable environment for cell adhesion and proliferation as shown in the MSCs study. However, the cell morphologic differences on the nanofibrous scaffold and

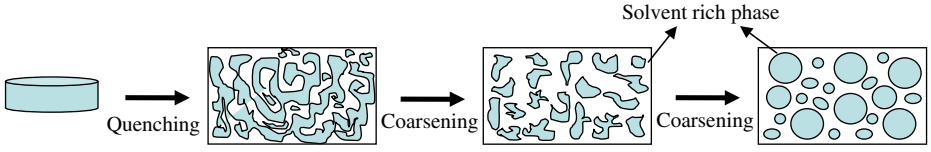

Fig. 11. Schematic illustration of phase separation processing.

platelet-like scaffold were small in the late period post-seeding, thus other quantificational detections should be employed to study the influence of substrate on MSC functions and cell–matrix interactions.

5. Conclusions

PLLA nanofibrous scaffolds with 3D macro/microporous structures were fabricated by liquid–liquid phase separation from a PLLA/dioxane/water ternary system. Macro/micropores formed by the crystals of dioxane/water and sequent evaporation could be controlled by the coarsening process. The walls between the micropores were nanofibrous network with the fiber diameter ranging from 50 nm to 200 nm. The nanofibrous structure was found to be influenced by coarsening parameters to a great extent. α' form crystal appear in the nanofibrous scaffold, while α form crystal was found in the platelet-like structure. Nevertheless, crystalline kinetics and crystalline morphology of PLLA in various solvents at different gelation temperatures should be investigated in detail. At last, SEM and MTT assay indicated that the nanofibrous scaffold provided a good environment for MSCs attachment and viability *in vitro*.

Acknowledgements

The authors would like to acknowledge the financial support by the National Natural Science Foundation of China (grants 50673102 and 30771143).

References

[1] Zhang Y, Zhang M. J Biomed Mater Res 2002;61:1.
[2] Ma PX, Choi JW. Tissue Eng 2001;7:23.
[3] Nguyen KT, West JL. Biomaterials 2002;23:4307.
[4] Chen GP, Ushida T, Tateishi T. Macromol Biosci 2002;2:67.
[5] Nair LS, Cato LT. Prog Polym Sci 2007;32:762.
[6] Mikos AG, Thorsen AJ, Czerwonka LA, Bao Y, Langer R, Winslow DN, et al. Polymer 1994;35:1068.
[7] Laurencin CT, El-Amin SF, Ibim SE, Willoughby DA, Attawia M, Allcock HR, et al. J Biomed Mater Res 1996;30:133.
[8] Mooney DJ, Baldwin DF, Suh NP, Vacanti JP, Langer R. Biomaterials 1996;17:1417.
[9] Whang K, Thomas CH, Healy KE. Polymer 1995;36:837.
[10] Park A, Wu B, Griffith LG. J Biomater Sci Polym Ed 1998;9:89.
[11] Lee KW, Wang SF, Fox BC, Ritman EL, Yaszemski MJ, Lu LC. Biomacromolecules 2007;8:1077.
[12] Lee KW, Wang SF, Lu LC, Jabbari E, Currier BL, Yaszemski MJ. Tissue Eng 2006;12:2801.
[13] Lo H, Ponticiello MS, Leong KW. Tissue Eng 1995;1:15.
[14] Nam YS, Park TG. J Biomed Mater Res 1999;47:8.
[15] Flemming RG, Murphy CJ, Abrams GA, Goodman SL, Nealey PF. Biomaterials 1999;20(6):573.
[16] Hua FJ, Kim GE, Lee JD, Son YK, Lee DS. J Biomed Mater Res Appl Biomater 2002;63:161.
[17] Smith LA, Ma PX. Colloids Surf B 2004;39:125.
[18] Barnes CP, Sell SA, Boland ED, Simpson DG, Bowlin GL. Adv Drug Delivery Rev 2007;59:1413.
[19] Ma PX, Zhang RY. J Biomed Mater Res 1999;46:60.
[20] Yang F, Murugan R, Ramakrishna S, Wang X, Ma YX, Wang S. Biomaterials 2004;25:1891.
[21] Woo KM, Chen VJ, Ma PX. J Biomed Mater Res 2003;67A:531.
[22] Woo KM, Jun JH, Chen VJ, Seo J, Baek JH, Ryoo HM, et al. Biomaterials 2007;28:335.
[23] Li XT, Zhang Y, Chen GQ. Biomaterials 2008;29:3720.
[24] Li SR, Carrubba VL, Piccarolo S, Sannino D, Brucato V. Polym Int 2004;53:2079.
[25] Ma PX, Zhang RY. J Biomed Mater Res 2000;52:430.
[26] Hu YH, Grainger DW, Winn SR, Hollinger JO. J Biomed Mater Res 2002;59:563.
[27] Hua FJ, Park TG, Lee DS. Polymer 2003;44:1911.
[28] Song SW, Torkelson JM. Macromolecules 1994;27:6389.
[29] Lee IC, Cheng LP, Young T. J Biomed Mater Res 2005;76A:842.
[30] Yasuniwa M, Tsubakihara S, Iura K, Ono Y, Dan Y, Takahashi K. Polymer 2006;47:7554.
[31] Kawai T, Rahman N, Matsuba G, Nishida K, Kanaya T, Nakano M, et al. Macromolecules 2007;40:9463.
[32] Hou QP, Grijpma DW, Feijen J. J Biomed Mater Res Part B Appl Biomater 2003;67B:732.
[33] Tu CF, Cai Q, Yang J, Wan YQ, Bei JZ, Wang SG. Polym Adv Technol 2003;14:565.
[34] Wei GB, Ma PX. Biomaterials 2004;25:4749.
[35] Liu XH, Won YJ, Ma PX. Biomaterials 2006;27:3980.
[36] Ma PX. Mater Today 2004;7:30.
[37] Nam YS, Park TG. Biomaterials 1999;20:1783.
[38] Kiefer J, Hedrick JL, Hilborn JG. Adv Polymer Sci 1999;147:161.
[39] Inoue T. Prog Polym Sci 1995;20:119.
[40] Lloyd DR, Kim SS, Kinzer KE. J Membr Sci 1991;64:1.
[41] Ji GL, Zhu BK, Cui ZY, Zhang CF, Xu YY. Polymer 2007;48:6415.
[42] Wang YM, João F. Eur Polymer J 2005;41:2335.